J Therm Spray Tech (2020) 29:1910–1925
https://doi.org/10.1007/s11666-020-01106-6

PEER REVIEWED

Fabrication of Metal Matrix Composites via High-Speed Particle Implantation

Ju Zhou[1] · Chang-Jiu Li[1] · Cheng-Xin Li[1]

Submitted: 20 April 2020 / in revised form: 6 September 2020 / Accepted: 29 September 2020 / Published online: 12 October 2020

Abstract This study deals with the improvement of the wear resistance of aluminum alloys by metal matrix composites (MMCs). The latter were fabricated by implanting high-speed solid particles into the metal surfaces. For that, stainless steel and Fe-based amorphous alloy particles were accelerated to the substrates using high-pressure nitrogen. The effect of multi-particle implantation, particle material properties and kinetic energy at impact, and pre-heating treatment of the substrate on particle implantation was investigated using numerical simulation. In addition, the effect of particle size on the MMCs microstructure, wear resistance, strengthening mechanism, and relative hardness was studied. The results showed that the method simultaneously achieved shot peening and metal matrix composite strengthening, that is, resulted in a double-strengthening effect. Furthermore, high-speed particle implantation effectively improved the wear resistance of the substrate: The wear volume of Fe-based amorphous alloy/Al MMCs was 5% of the untreated aluminum substrate and that of stainless steel/Al MMCs 14–44%. It is believed that laser-assisted particle implantation can be used to efficiently increase the thickness and surface properties of MMCs.

Keywords aluminum alloys · double-strengthening effect · high-speed particle implantation · laser-assisted particle implantation · metal matrix composites (MMCs)

✉ Cheng-Xin Li
licx@mail.xjtu.edu.cn

[1] State Key Laboratory for Mechanical Behavior of Materials, School of Materials Science and Engineering, Xi'an Jiaotong University, Xi'an 710049, Shaanxi, People's Republic of China

Introduction

Aluminum and its alloys have excellent physical properties, such as low specific gravity, high specific strength, good cutting, hot workability, non-magnetic and electromagnetic shielding properties, no adverse effects on the environment, and high recovery rates. In addition, aluminum is chemically active due to its small electrode potential and oxidation reactions occur easily, forming an aluminum oxide film that provides aluminum with good corrosion resistance. Hence, aluminum and its alloys are widely used in aviation, aerospace, marine, construction, automotive, energy chemical, packaging, electronic, weapons, and other fields (Ref 1–4).

However, the poor wear resistance and high friction coefficient of aluminum alloys completely limit their application. In practical engineering applications, many types of mechanical parts fail before reaching their designed service life owing to fatigue, friction, wear, and other problems. Through investigation, it was found that the failure of a large number of metal structural parts occurred mostly at their surface (Ref 5, 6). Therefore, the use of numerous surface treatment technologies to improve the friction, wear, and corrosion resistance of the surface of metal components, thus ensuring the long-term standard, safe operation, and extended service life of large machinery and equipment, is of great practical significance for industrial production.

At present, the methods for improving the wear resistance of aluminum and its alloys predominantly include metal matrix composites (MMCs) (Ref 7, 8), surface coating treatment methods (microarc oxidation, anodizing, chemical conversion, electroplating, laser cladding, thermal spraying, etc.) (Ref 9), surface deformation strengthening (shot peening, rolling strengthening, and extrusion

strengthening) (Ref 10–12), and surface phase strengthening (laser, electron beam, induction heating surface hardening, etc.) (Ref 13). These technologies not only retain the excellent properties of aluminum alloy but also provide some new properties to aluminum alloys, allowing a more extensive range of application. However, there are still some restrictions. For example, the process of manufacturing MMCs by adding hard particles into a metal matrix is both complex and challenging and requires a significant amount of time and economical provision (Ref 14). Therefore, obtaining MMCs coatings on the just substrate surface is problematic. The use of common metal material surface treatment processes, such as microarc oxidation, anodization, chemical conversion film treatment, electroplating, laser cladding, vapor deposition, and thermal spraying, improves the wear resistance of metal materials; however, the thickness of the film or the mechanical properties of the coating limit its application. Furthermore, these methods necessitate some environmental contamination. Therefore, there is a vital necessity for an efficient, low-cost, simple, and environmentally friendly surface strengthening method to improve the surface properties of metal materials and increase their wear resistance.

In traditional cold spray, MMCs layer was fabricated by spraying composite powder on a substrate to form coating (Ref 15–17). Before spraying, the composite powder was synthesized via in situ reaction followed by gas-atomization process (Ref 17) or mechanically blended (Ref 15, 16). In this study, a MMCs protective layer was prepared on the surface of the metal substrate via high-speed particle implantation. By modulating the parameters of cold spraying and using high-pressure gas to accelerate the hard particles, high-speed hard particles were implanted into the metal substrate material, forming MMCs without developing a coating. The hard particles were accelerated via a supersonic, high-pressure gas flow generated by a de Laval nozzle; the particles were emitted from the axial direction of the nozzle into the supersonic flow, obtaining the required high speeds. The high-speed particles were implanted into the substrate after impacting its surface; a high-hardness wear-resistant MMCs layer with uniform hard particles was thus prepared on the surface of the metal substrate. During the preparation process, the particles did not undergo obvious heat treatment; hence, oxidation and the consequential structural changes did not occur (Ref 18). During the formation of MMCs, high-speed particles were implanted into the metal substrate, resulting in a strong impact on the substrate and causing severe plastic deformation of the substrate surface. The dislocation density and value increase during the plastic deformation process, caused by dislocation cross-slip, dislocation climb, and new grain growth, which significantly improves the surface hardness of the substrate and plays a role in shot peening (Ref 19). And beneficial residual compressive stress can be introduced in the particle implantation process, which effectively improves the fatigue wear resistance and fatigue life of the metal substrate (Ref 20, 21). In addition, the formed MMCs are strengthened via the introduction of reinforcing phase particles. Therefore, the method of preparing MMCs on the metal substrate surface via high-speed particle implantation simultaneously achieves shot peening and metal matrix composite strengthening, thereby doubling the strengthening effect.

In this study, the process of implanting hard particles into the surface of the metal substrate and forming MMCs was rapid; the process of preparing the MMCs with a volume of 50 mm × 50 mm × 100 μm lasted 2 s and the substrate remained solid without melting during particle implantation. Therefore, the preparation method was simple and efficient and consequently time saving and inexpensive. In addition, no solution was involved throughout the process and the accelerating gas used was an inert gas that does not pollute the environment. The remaining reinforced powder could be recycled, which conforms to the scientific concept of environmental sustainability. In addition, MMCs were formed only on the surface of the substrate and with minimal mass increase, which is beneficial for taking complete advantage of aluminum alloy's light weight.

In this study, to investigate the influence of the relative hardness between the hard particles and the substrate on the microstructure and wear resistance of MMCs, 316L stainless steel and Fe-based amorphous alloy particles with different hardness values were used. In addition to the aluminum substrate, a lead metal with low hardness was used as the reference term. The effects of the particle size and surface density of hard particles were also investigated. In addition, the effects of multi-particle implantation, the particle's material properties, the kinetic energy of the particles, and pre-heat treatment of the substrate were studied using numerical simulation. Furthermore, laser-assisted particle implantation was used to increase the MMCs thickness.

Experimental Details

Materials

316L stainless steel and Fe-based amorphous alloy particles were used for implantation, as shown in Fig. 1. The detailed size distribution of the 316L stainless steel and Fe-based amorphous alloy powders is shown in Fig. 2. An aluminum and lead sheet were used as the substrate, and the sheet was grounded (using P120 and P220 grit), polished, and subsequently cleaned using acetone.

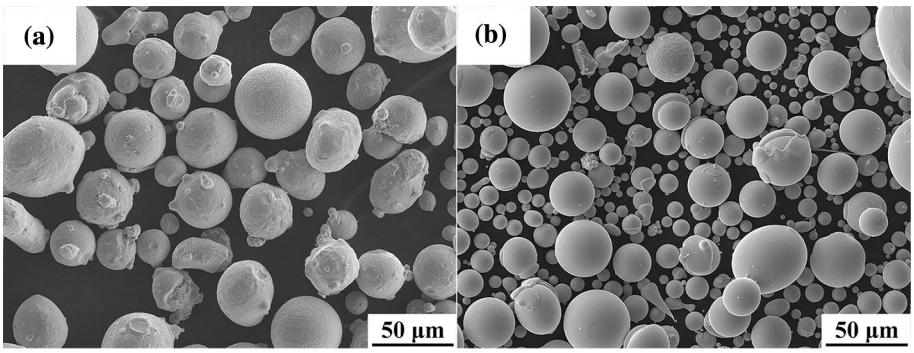

Fig. 1 SEM micrographs of particles: (a) 316L stainless steel, (b) Fe-based amorphous alloy

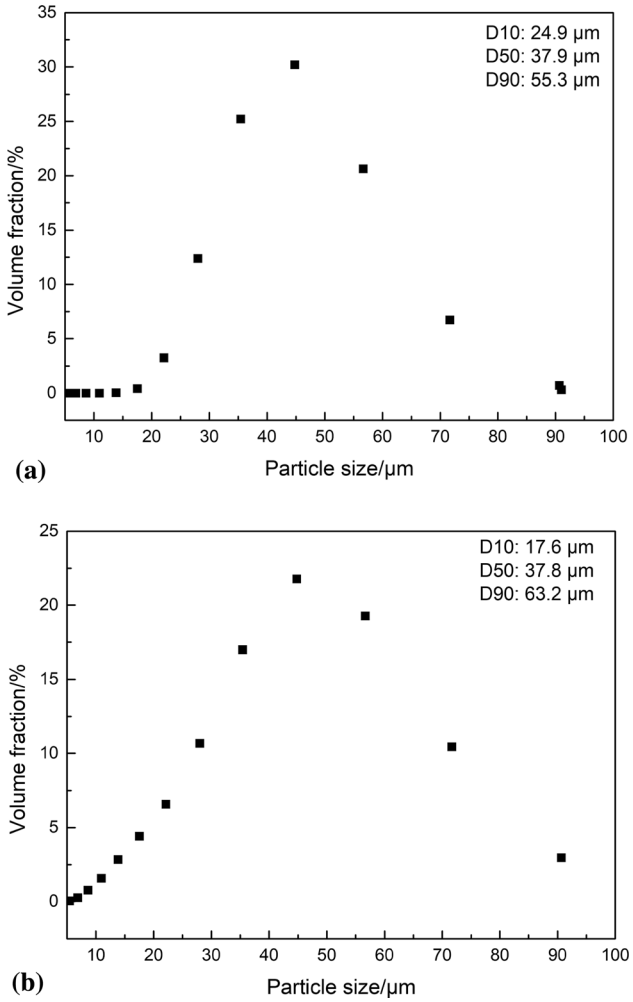

Fig. 2 Size distributions of powder: (a) 316L stainless steel, (b) Fe-based amorphous alloy

Particle Acceleration System

The particles were accelerated using a high-pressure gas. In this study, high-speed particle implantation was achieved using an atmospheric cold-spraying system (CS2000, Xi'an Jiaotong University, China). Implantation particles were accelerated in a de Laval nozzle using high-pressure nitrogen gas. After particles underwent acceleration via the high-speed gas flow through the nozzle, the particle velocity in the throat of the nozzle was comparable to the speed of sound. After passing through the throat of the nozzle, the particle velocity continued to increase, achieving a high velocity before impacting the substrate. In this study, the carrier gas was nitrogen (N_2). The gas pressure and temperature were maintained at 4 MPa and 400 °C, respectively. The stand-off distance from the nozzle exit to the substrate surface was 20 mm. During particle implantation the spray gun traversed only once, at a speed of 800 mm/s relative to the substrate. The particle implantation parameters are presented in Table 1.

Table 1 Particle implantation parameters

Parameter	Value	Unit
Gas pressure	4	MPa
Gas temperature	400	°C
Stand-off distance	20	mm
Powder feeding rate	5.2, 10.4, 15.6	g/min
Nozzle scanning velocity	800	mm/s
Spray passes	1	Time

Analysis of Microstructure and Properties

The morphologies of the initial 316L stainless steel particles, Fe-based amorphous alloy particles, and MMCs were examined using scanning electron microscopy (SEM, TESCANMIRA 3 LMH, Czech) (Ref 22). The hardness of the MMCs was measured from the polished cross section using the Vickers microhardness test, under a load of 10 g and a dwelling time of 10 s per sample.

The MMCs and untreated aluminum substrate were subjected to ball-on-disk-type wear tests, with Si_3N_4 balls used as friction pairs. The wear test conditions are presented in Table 2. The morphology of the wear tracks was observed via scanning electron microscopy. The 3D morphologies of the wear tracks, depth, and width of the slot

Table 2 Wear test condition in this study

Ball material	Si_3N_4
Load on the ball	300 g (2.94N)
Scratching shape	Circle (5 mm diameter)
Scratching speed	100 mm/s
Revolution	8500 r

created by the wear test were performed using a color 3D laser scanning microscope. The wear volume was calculated as follows (Ref 23):

$$W_v = \frac{t}{6b}\left(3t^2 + 4b^2\right) \times 2\pi r$$

where W_v is the wear volume and *t, b,*, and *r* are the depth, width, and radius of the wear tracks, respectively (Ref 23).

Numerical Simulation of Particle Implantation

The explicit finite element analysis software ABAQUS was used to simulate the implantation behavior of a single particle (Ref 24, 25). The Euler algorithm was used for the solution, based on the basic mass, momentum, and energy conservation equations. Spherical particles 30 μm in diameter were used. The ABAQUS software does not support the Euler algorithm in two dimensions; hence, a slice with a thickness of (1/20) d_p (where d_p represents the particle diameter) of the entity model was set in the Eulerian model, and the calculated outputs were varied with element size. In this study, the element and grid size of (1/100) d_p (Ref 26) were used, considering the convergence and stability of simulations (Ref 27). A 3D Eulerian coupled temperature–displacement eight-node element (EC3D8RT) (Ref 26) was used in meshing, which considered the heat conduction that occurred during the particle implantation process. The dynamic temperature–displacement explicit was used in this study, which considered heat conduction. In this model, the degrees of freedom in the z-direction were constrained for all elements, the bottom and right sides of the model were fixed, and the displacement of the left side of the model was constrained in the x-direction (Ref 26–28), as shown in Fig. 3.

The material deformation of the particle and the substrate was described using the Johnson–Cook plasticity model (Ref 29), which considers the effects of strain rate hardening, strain hardening, and thermal softening (Ref 27, 29). The stresses were designated according to the von Mises plasticity model (Ref 27, 30, 31). The yield stress (σ_y) can be expressed as follows (Ref 27):

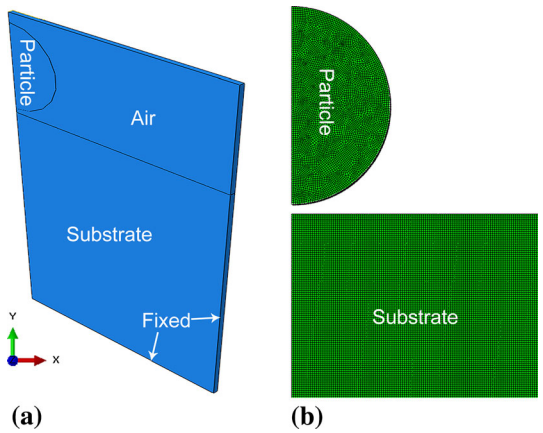

Fig. 3 (a) Symmetric model and computational domain of particle (30 μm) implanting into aluminum substrates under the Eulerian frame and (b) the enlarged view of mesh

$$\sigma_y = (A + B\varepsilon^n)\left[1 + C\ln\left(1 + \frac{\dot{\varepsilon}}{\dot{\varepsilon}_0}\right)\right]\left(1 - \left[\frac{T - T_{room}}{T_{melt} - T_{room}}\right]^m\right) \quad \text{(Eq 1)}$$

where ε and $\dot{\varepsilon}$ are the equivalent plastic strain and strain rate, respectively; $\dot{\varepsilon}_0$ is the reference strain rate; and *A*, *B*, *n*, *C*, and *m* are material-dependent constants. In more detail, *A* is the yield stress in a quasi-static simple tension or compression test, *B* is the strain-hardening parameter, *C* is the dimensionless strain rate-hardening coefficient, and T_{room} and T_{melt} are the reference temperature and melting point, respectively (Ref 32, 33).

Results and Discussion

Simulation of Particle Implantation

The properties of materials, such as yield strength, elastic modulus, hardness, and Poisson's ratio, have important effects on the deformation ability of the material (Ref 34). The yield strength and hardness represent the material's ability to resist plastic deformation, while the elastic modulus and Poisson's ratio reflect the material's ability to resist elastic deformation (Ref 35). The degree of deformation of the substrate has a significant impact on the particle implantation effect. Preceding numerical and experimental studies (Ref 25, 36, 37) have found that the initial kinetic energy of a particle is mostly dissipated owing to the plastic deformation of the relatively soft counterpart during the impact between the hard and soft materials. Some experimental and numerical studies of particle impacting (Ref 38) have found that the initial kinetic energy of particles has a great impact on the deformation of the particles and substrate during the

particle implantation process. Bae et al. (Ref 37) found that during the particle impact process the initial kinetic energy of the particles will be converted into plastic dissipation (E_P), viscous dissipation (E_V), recoverable elastic strain (E_R), and frictional dissipation energy (E_F). Viscous effects and frictional work are relatively small compared to the plastic dissipation energy and hence can be ignored. Therefore, the initial kinetic energy of the impacting particle mainly dissipates via the plastic deformation of the particle and substrate. Accordingly, the initial kinetic energy of the particles affects the plastic deformation of the material and thus greatly affects the implantation of the particles (Ref 38).

Effect of Material Properties of Particles

In order to verify the effects of various material properties of the particles on particle implantation, the process of implantation of different particles into the aluminum substrate was simulated. The material properties are listed in Table 3. The velocity of the particle was 431.53 m/s. The particle diameter was 30 μm. The deformation of the particle was characterized using the compression ratio (R_c), which is defined as (Ref 39):

$$R_c = \frac{d_p - h_p}{d_p} \times 100\% \quad \text{(Eq 2)}$$

where d_p is the original particle diameter and h_p is the height of the deformed particle in the direction of implantation.

When the particle material properties are different, the degree of deformation of the particles, the substrate, and the particle implantation depth are also different, as shown in Fig. 4. This indicates that the deformation of WC-Co, TC4, Ti, and 316L stainless steel particles is particularly small after being implanted into the aluminum substrate. The yield strengths of these materials are relatively high, and hence, the ability to resist deformation is relatively large (Ref 35). The hardness of Cu and Ni is also relatively high; however, owing to their low yield strength, it was found that the degree of deformation of Cu and Ni was comparatively large after particle implantation, indicating that the yield strength had a greater effect on deformation than hardness.

After the particles were implanted into the Al substrate, it was found that TC4, Ti, and 316L stainless steel particles had a similar degree of deformation; however, the deformation degrees of the Al substrate were moderately different. In the 316L/Al case, the Al substrate deformation

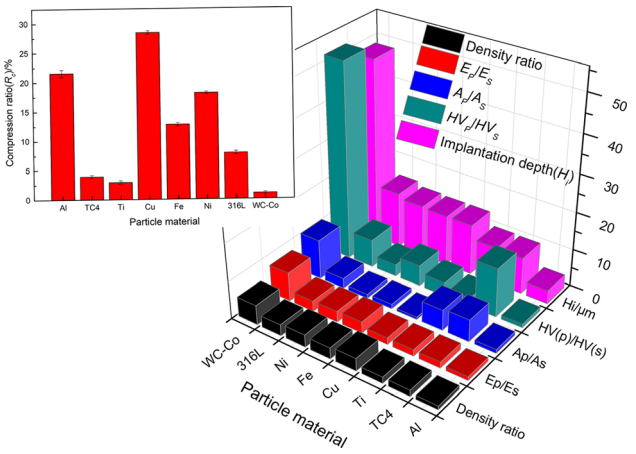

Fig. 4 The effect of material properties on the particle implantation depth: H_i(particle implantation depth), density ratio ($\text{Density}_{\text{particle}}/\text{Density}_{\text{substrate}}$), HV_P/HV_S($\text{Hardness}_{\text{particle}}/\text{Hardness}_{\text{substrate}}$), A_P/A_S($\text{Yield strength}_{\text{particle}}/\text{Yield strength}_{\text{substrate}}$), E_P/E_S($\text{Elastic modulus}_{\text{particle}}/\text{Elastic modulus}_{\text{substrate}}$)

Table 3 Simulation parameters (Ref 25, 40–42)

Parameter	Al	316L SS	WC-Co	Ni	Fe	Cu	Ti	TC4
Density, kg/m^3	2700	8031	14,000	8900	7890	8960	4510	4428
Thermal conductivity, W/ (kg m °C)	220	16	63	88.5	46.5	386	17	7.9
Specific heat, J/ (kg °C)	920	457	293	446	452	383	528	580
Melting point, °C	620	1368	1495	1455	1535	1083	1650	1605
Elasticity modulus, GPa	68	193	527	200	207	120	116	114
Poisson's ratio	0.36	0.3	0.25	0.31	0.29	0.34	0.34	0.34
A, MPa	148	388	1550	163	175	90	806	862
B, MPa	346	1728	22,000	648	388	292	481	331
N	0.183	0.8722	0.45	0.33	0.32	0.31	0.319	0.34
C	0.183	0.02,494	0.016	0.006	0.06	0.025	0.019	0.012
M	0.86	0.6567	1	1.44	0.55	1.09	0.655	0.8

was severe and the particle implantation depth was 15 μm. However, the deformations of the Al substrate were slight in the TC4/Al and Ti/Al cases and the particle implantation depths were only 9.7 and 9.8 μm. This demonstrated that the initial kinetic energy of the particles had a particularly large impact on the particle implantation. 316L stainless steel had a higher density and greater kinetic energy at the same particle velocity. During the particle implantation process, more kinetic energy can be converted into plastic dissipative energy of the substrate, causing more severe plastic deformation of the aluminum substrate and thereby promoting particle implantation (Ref 38).

In the case of Cu/Al and Fe/Al, the particle implantation depths were the same but the degree of particle deformation was different. The analysis found that the hardness, elastic modulus, and yield strength of the Cu particles were lower than those of Fe. Therefore, the degree of deformation of the Cu particles was greater than that of Fe during the particle implantation process (Ref 38, 43). However, Cu has a higher density than Fe and thus more kinetic energy was converted into plastic dissipative energy of the substrate, causing more severe plastic deformation of the aluminum substrate. The hardness, elastic modulus, and yield strength of Fe were high, particle deformation was slight, and substrate deformation was severe, which ultimately resulted in the same implantation depth in the two cases.

After the WC-Co particles were implanted into the aluminum substrate, it was found that the substrate underwent more severe deformation, the particles only slightly deformed, and the particle implantation depth was approximately 49 μm. The WC-Co particles had the highest density and hence the largest kinetic energy at the same particle velocity. The hardness, elastic modulus, and yield strength of the WC-Co particles were the highest. During the particle implantation process, the resistance of the particles to deformation increased (Ref 35). Therefore, more kinetic energy was converted into plastic dissipative energy of the soft Al substrate and the substrate was severely deformed; this promoted the implantation of the particles, indicating that WC-Co/Al achieved the largest implantation depth (Ref 38, 43).

In order to quantitatively analyze the effects of various material properties and the initial energy of particles on the particle implantation effect, particle implantation was simulated. The results are as follows: Under the same conditions, as the yield strength of the substrate increased, it was found that the degree of deformation of the substrate decreased and the particle implantation depth decreased. The substrate's ability to resist plastic deformation increased as the yield strength of the substrate increased (Ref 35), and consequently, the degree of plastic deformation of the substrate decreased under the same load. As shown in Fig. 5(a), with an increase in the yield strength of the substrate, the plastic dissipative energy of the substrate decreased, while the plastic dissipative energy of the particles increased. Therefore, the degree of deformation of the substrate decreased and the degree of deformation of the particles increased, resulting in a decrease in the particle implantation depth. Figure 5(b) shows the influence of the elastic modulus on particle implantation. It was found that as the elastic modulus of the substrate increased, the degree of plastic deformation of the substrate decreased, causing the particle implantation depth to decrease. Because the substrate's elastic modulus increased under the same stress condition, the substrate's resistance to deformation increased and the degree of deformation was

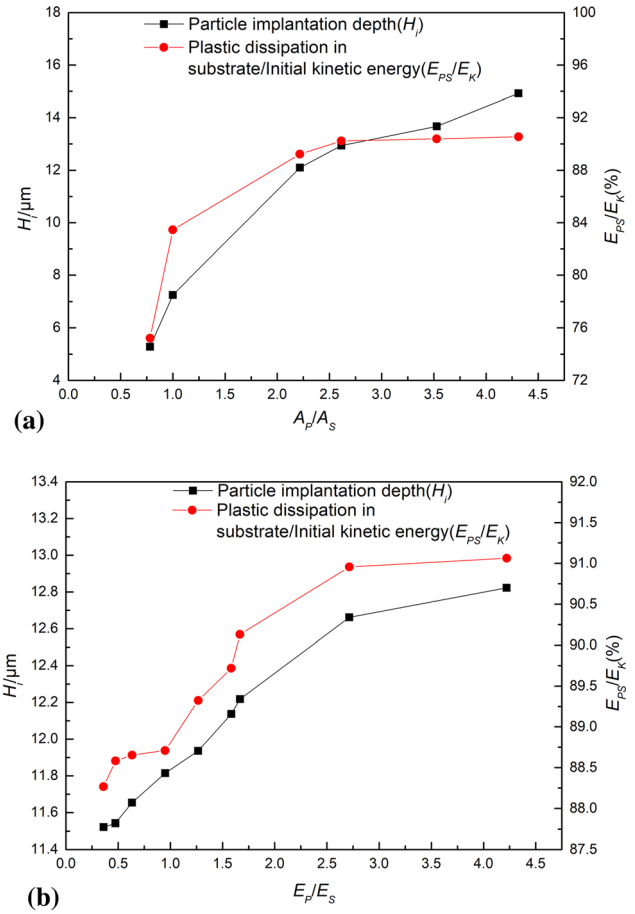

Fig. 5 The effect of yield strength and elastic modulus on particle implantation depth and E_{PS}/E_K(plastic dissipation energy/initial kinetic energy): (a) A_P/A_S($\text{Yield strength}_{\text{particle}}/\text{Yield strength}_{\text{substrate}}$); (b) E_P/E_S($\text{Elastic modulus}_{\text{particle}}/\text{Elastic modulus}_{\text{substrate}}$)

reduced, which further hindered the implantation of particles (Ref 35).

Effect of Particle Kinetic Energy

In order to further explore the effects of particle kinetic energy on particle implantation depth, the implantation process of the particles was simulated. The particles and substrate were 316L stainless steel and aluminum alloy, respectively. The effect of kinetic energy was determined by varying the particle velocity. As a result, it was found that under otherwise consistent conditions, as the particle velocity increased the degree of deformation of the substrate became increasingly severe and the degree of particle deformation increased simultaneously, resulting in an increase in the particle implantation depth, as shown in Fig. 6. This is because the increase in particle implantation velocity indicates a greater kinetic energy. During the particle implantation process, the particles and the substrate can absorb more energy, which is conducive to subsequent plastic deformation. Therefore, more plastic dissipation energy in the substrates leads to severe plastic deformation of the substrate (Ref 38), promoting particle implantation and causing an increase in the particle implantation depth, as shown in Fig. 6.

The Effect of Preheating of Substrate and Multi-particle Implantation

After the aluminum substrate was subjected to pre-heat treatment, it was found that the deformation of the substrate was significantly more severe and the particle implantation depth was significantly increased. After preheating the substrate, the substrate first became soft, the hardness was critically reduced, and hence the ability to resist plastic deformation was also reduced (Ref 44, 45). Subsequently, after the substrate was pretreated, the elastic modulus and yield strength of the substrate decreased (Ref 46). Under the same stress conditions, the deformation of the substrate increased. Therefore, after the substrate was preheated, the deformation of the substrate became more severe, which promoted particle implantation and resulted in an increase in particle implantation depth, as shown in Fig. 7(a).

The simulation found that the trend of the plastic dissipation energy in the substrate was different from the preceding one. As the preheating temperature of the substrate increased, the degree of deformation of the substrate increased, but the plastic dissipation energy decreased. The different trend of plastic energy dissipation was as follows: Plastic dissipation energy was generated due to the dissipation of plastic work during deformation (Ref 44, 45). When metals attain a thermal softening state, thermal softening will gradually eliminate work hardening. The greater the effect of thermal softening, the greater the degree of elimination of work hardening and hence less plastic workability is required for deformation. Therefore, after the substrate is preheated, it is easier for the substrate

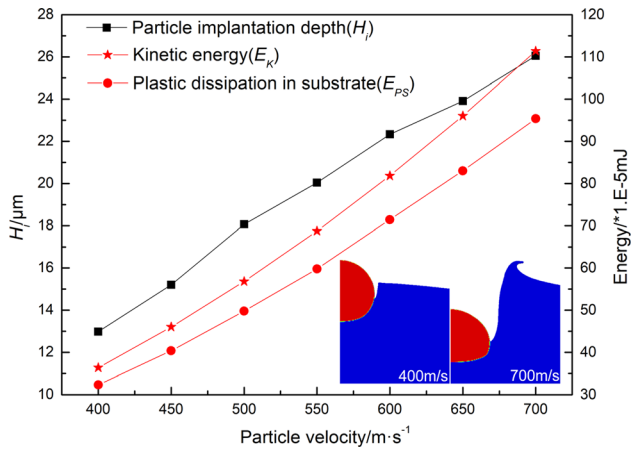

Fig. 6 The particle implantation depth and energy versus the particle implantation velocity

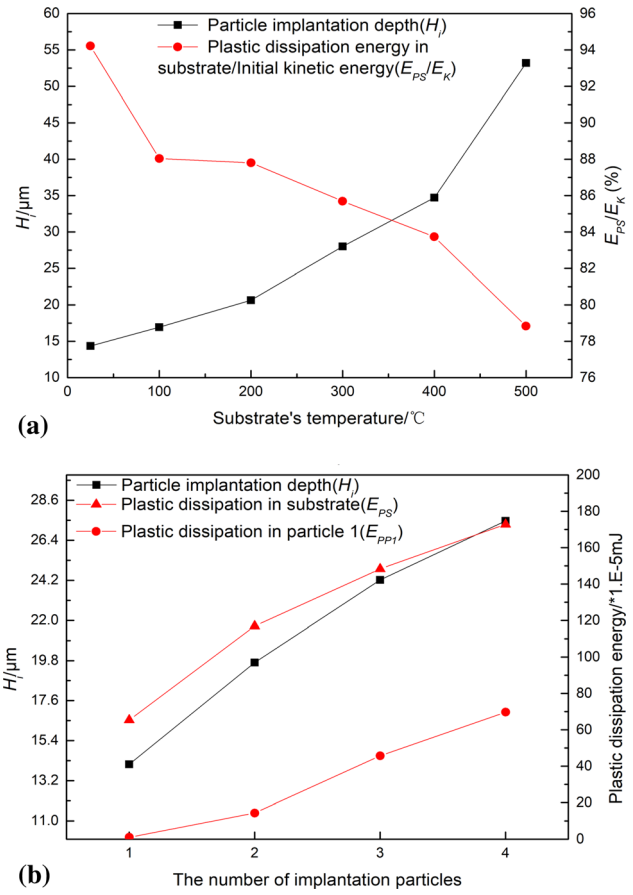

Fig. 7 The particle implantation depth and plastic dissipation energy versus (a) the substrate's temperature and (b) the number of implantation particles

to undergo thermal softening. Accordingly, relatively small plastic work can cause a relatively large plastic deformation (Ref 44, 45).

In order to verify the impact of the tamping effect on particle implantation, a numerical simulation was performed on the multi-particle implantation. It was revealed that as the number of implanted particles increased, the implantation depth of the particles showed an increasing trend, and the implantation of subsequent particles will have a tamping effect on previously implanted particles (Ref 47), as shown in Fig. 7(b). It is worth noting that the most severely deformed particle (marked particle 1) is near the substrate, which is mainly due to the subsequent impact of further particles (Ref 48, 49). More particles implantation leads to more severe the deformation of the particles 1. During the particles implantation, a quantity of the kinetic energy of the subsequent particles will be absorbed by the implanted particles and the substrate, causing them to undergo plastic deformation. The more particles implanted, the more energy will be absorbed by the implanted particles and the substrate. Therefore, more plastic dissipation energy can be used for plastic deformation, leading to a greater degree of deformation of particle 1 and substrate, resulting in a deeper particle implantation depth (Ref 27, 38), as shown in Fig. 7(b).

MMCs Characterization

Effect of Relative Hardness

1050 aluminum and pure lead metal with different hardness values were used as the substrate, and 316L stainless steel and Fe-based amorphous alloy powders, with different hardness values, were used as the implantation particles. The acceleration gas pressure and temperature were 4 MPa and 400 °C, respectively. The microstructure morphologies of the prepared MMCs are shown in Fig. 8. On the surface of the 316L/Al and Fe-based amorphous alloy/Al MMCs, some particles deteriorated and left behind empty pits; these were mostly large particles, as shown in Fig. 8(a) and (b). Prior numerical results (Ref 50) found that under consistent spraying conditions a larger particle diameter corresponds to a slower speed, which is not conducive to particle implantation. After particles were implanted into the surface of the lead metal, the hardness of the lead was extremely low and much smaller than that of the hard particles, thus increasing the susceptibility of the substrate to severe plastic deformation and thereby promoting the implantation of particles (Ref 37). It was found that severe plastic deformation occurred on the surface of the lead substrate after particle implantation; there was no shedding of the particles and the particles were successfully embedded in the substrate as a result of deep penetration,

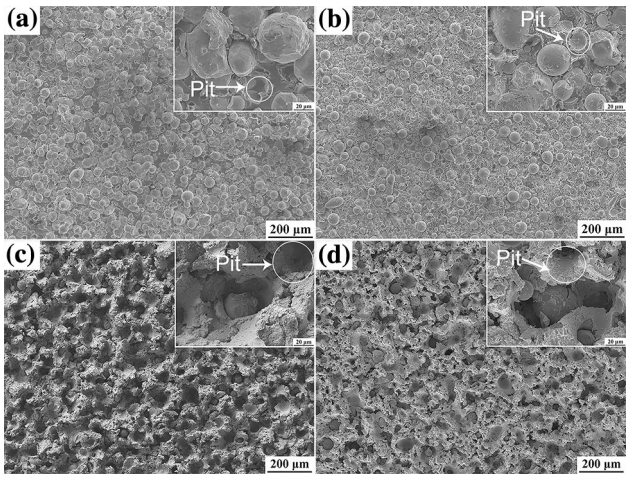

Fig. 8 SEM images of MMCs surface: (a) 316L/Al; (b) Fe-based amorphous alloy/Al; (c) 316L/Pb; (d) Fe-based amorphous alloy/Pb

resulting in a rough MMCs surface, as shown in Fig. 8(c) and (d).

Micromorphology analysis of the cross section of the MMCs revealed that after the hard particles were implanted into the substrate, MMCs were formed with uniform and dispersed distribution of the hard particles, as shown in Fig. 9. The particles were completely and tightly embedded in the substrate; this was because subsequent particles impacted the substrate, causing severe plastic deformation. Similarly, the heavy embedding of the particles made it difficult for them to shed (Ref 47). As shown in Fig. 9, when the hardness of the substrate was constant, as the hardness of the particles increased the number of implanted particles and the thickness of the MMCs increased. When the hardness of the particles was constant, as the hardness of the substrate decreased the number of implanted particles also greatly increased and the thickness of the MMCs increased. This is because hardness represents the material's ability to resist plastic deformation (Ref 43). When the particle hardness increased and the substrate hardness decreased, the particles could better resist plastic deformation, while the substrate's ability to resist plastic deformation decreased. The initial kinetic energy of a particle was mostly dissipated owing to the plastic deformation of the relatively soft counterpart (Ref 37, 43). Therefore, the substrate underwent severe plastic deformation, promoting the implantation of particles and further increasing the thickness of the MMCs.

Quantitative analysis of the relationship between the thickness of the MMCs and the relative hardness, ΔHV (the difference between the hardness of the particles and the substrate), found that when the substrate hardness was maintained (the Vickers hardness of the Fe-based amorphous alloy, 316L SS, Al, and Pb was 1401, 353, 43, and 7, respectively), and the particle hardness increased (ΔHV

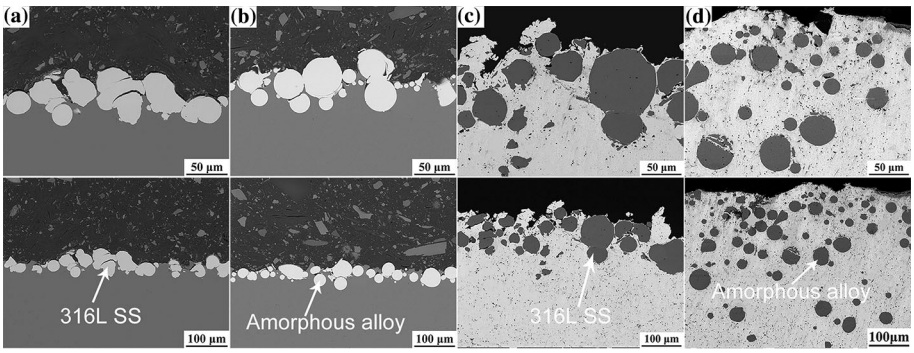

Fig. 9 SEM images of MMCs cross section: (a) 316L/Al; (b) Fe-based amorphous alloy/Al; (c) 316L/Pb; (d) Fe-based amorphous alloy/Pb

increased), and the thickness of the composite layer increased accordingly. When the particle hardness was the same, as the matrix hardness decreased (ΔHV increased), the thickness of the MMCs increased, as shown in Fig. 10. The degree of influence of the substrate hardness on the thickness of the MMCs was greater than that of the particle hardness.

Effect of Areal Density of Particles on MMCs Surface

In order to verify the effect of particle implantation and wear resistance on particle distribution on the surface of the MMCs, particle implantation experiments were carried out with different powder feeding rates. The powder feeding rates were 5.2 g/min, 10.4 g/min, and 15.6 g/min, respectively. The micromorphologies of the MMCs are shown in Fig. 11. It was found that when the powder feeding rate was relatively low, relatively few particles were implanted, the area of the bare substrate was large, and the particles were shed, leaving behind pits on the substrate surface, as shown in Fig. 11(a). With an increase in powder feeding rate, the number of implanted particles increased, the particle distribution on the surface of the MMCs was denser, and the area of the exposed substrate decreased, as shown in Fig. 11(b). When the powder feeding rate was further increased, the number of implanted particles was larger and there was a denser distribution of particles on the surface of the MMCs, completely covering the substrate, as shown in Fig. 11(c). Statistics on the areal density of the particles on the substrate surface revealed that the areal density of the particles increased with an increase in the powder feeding rate, as shown in Fig. 12.

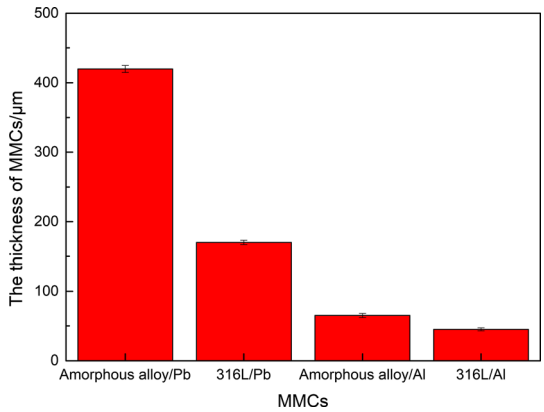

Fig. 10 The relationship between the thickness of the MMCs and the relative hardness ΔHV ($\Delta HV = Hardness_{Particle} - Hardness_{Substrate}$)

Effect of Particle Size of Hard Particles

The acceleration effect of 316L stainless steel particles with different diameters under the same gas temperature and pressure was simulated using a computational fluid dynamics model (Ref 51). It was found that under the same acceleration conditions, a larger particle diameter resulted in a smaller particle velocity (Ref 50). After calculating the kinetic energy, it was found that although the velocity of the particles decreased, the kinetic energy of the particles increased with an increase in particle size, as shown in Fig. 13. A numerical simulation of the particle implantation process determined that as the particle diameter increased, the particle implantation depth also increased. Under the same acceleration conditions, as the diameter of the particles increased, the kinetic energy of the particles increased. During the particle implantation process, more kinetic energy was converted into plastic dissipation energy of the substrate. The substrate had more energy for plastic deformation and severe plastic deformation occurred, which promoted the implantation of particles so that the particle implantation depth increased with the increase in particle diameter, as shown in Fig. 13.

In order to verify the precision of the simulation results, 316L stainless steel particles with different particle diameters were used for the particle implantation experiments. It was found that when the particle diameter was relatively small, the number of implanted particles was relatively large and the depth of the MMCs was approximately 160 μm, as shown in Fig. 14. When large-sized particles were used for the implantation experiment, the acceleration effect of the large particles was reduced under consistent accelerated gas conditions and the obtained velocity was

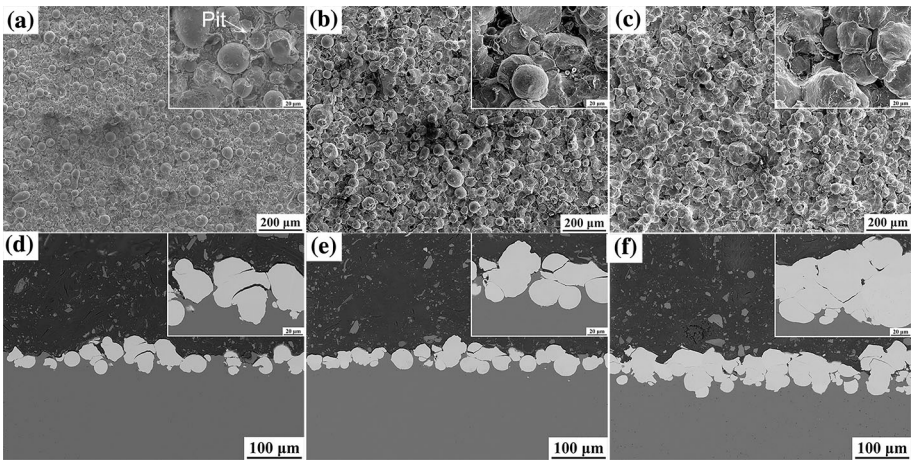

Fig. 11 SEM images of 316L/Al MMCs with different power feeding rates: (a) and (d) 5.2 g/min; (b) and (e) 10.4 g/min; (c) and (f) 15.6 g/min

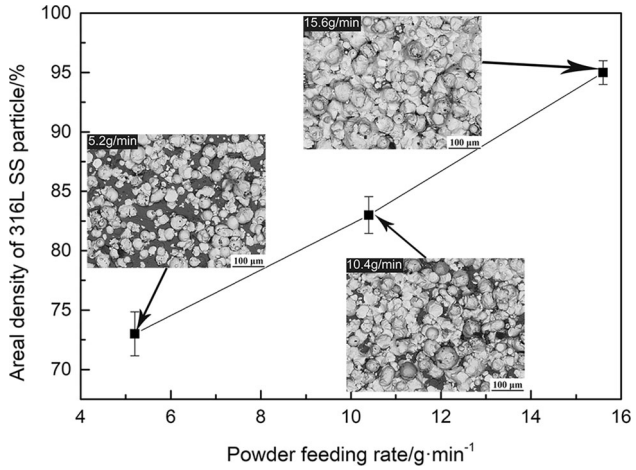

Fig. 12 Areal density of 316L SS particle as a function of powder feeding rate

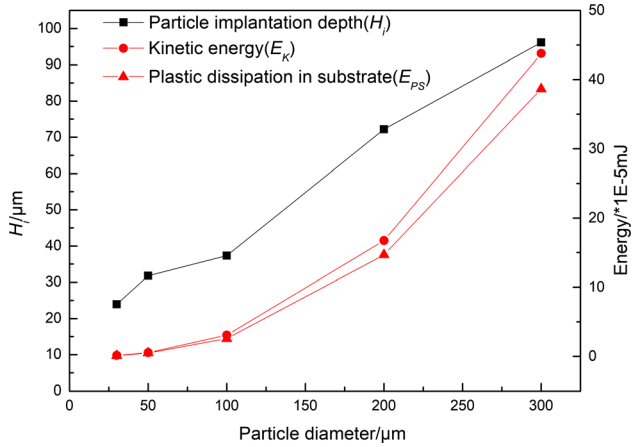

Fig. 13 The particle implantation depth and energy versus the particle diameter

relatively small, resulting in an increased probability of particles shedding during the implantation process; hence, the number of particles in the substrate decreased. However, because of the relatively large kinetic energy of large-sized particles, more kinetic energy was converted into the plastic dissipation energy of the substrate during the particle implantation process and the substrate underwent more severe plastic deformation, thereby promoting particle implantation. Therefore, the thickness of the MMCs increased to approximately 320 μm.

Wear Behavior

Microhardness Values

The hardness test was performed on the MMCs and an untreated aluminum substrate. It was found that the hardness of the Fe-based amorphous alloys/Al MMCs was $400 \leq HV_{Amorphousalloys/Al} \leq 1300$, the hardness of the 316L/Al MMCs was $100 \leq HV_{316L/Al} \leq 450$, and the hardness of

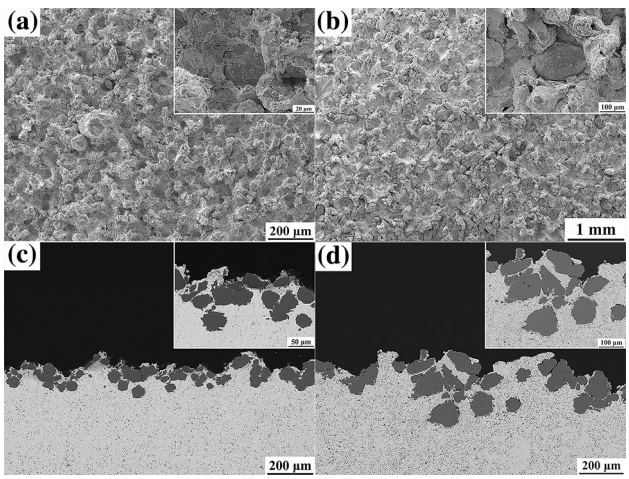

Fig. 14 SEM images of MMCs: (a) small-size 316L SS particles, 316L/Al MMCs, surface; (b) large-size 316L SS particles, 316L/Al MMCs, surface; (c) small-size 316L SS particles, 316L/Al MMCs, cross section; (d) large-size 316L SS particles, 316L/Al MMCs, cross section

the untreated aluminum substrate was approximately $HV_{Al} = 43$. After the hard particles were implanted, the microhardness of the aluminum substrate significantly improved. The increase in hardness was due to the effects of the hard particle implantation and tamping effect. First, the hardness of the MMCs could be significantly improved by implanting high-hardness Fe-based amorphous alloy and 316L stainless steel particles. In addition, during the implantation of hard particles, the hard particles strongly impacted the aluminum substrate, which caused strong plastic deformation and induced work-hardening effects (Ref 19, 22, 52). This was due to cross-slip of the dislocations, dislocation climbing, and new grain growth, which led to an increase in dislocation density and number of dislocations (Ref 53). Therefore, the microhardness of the near-surface region increased significantly (Ref 52). In addition, further implantation of hard particles resulted in severe plastic deformation of the substrate and the generation of more dislocations; the depth of the hardness enhancement zone also increased. The higher the hardness of the implanted particles, the greater the hardness of the MMCs formed.

Wear Resistance

To evaluate the wear behavior of the MMCs, ball-on-disk wear tests were conducted. The results obtained for the MMCs and bare aluminum were then compared. As shown in Figs. 15 and 16, the depth, width, and wear volume of the wear tracks on the aluminum substrate decreased sharply after the implantation of the hard particles. It was found that the MMCs formed by implanting a hard Fe-based amorphous alloy were most resistant to wear, with the narrowest wear tracks and the smallest wear volume (Ref 23, 53, 54). The untreated aluminum substrate underwent severe wear, with the widest wear tracks, and the wear volume was approximately 19 times greater than that of the Fe-based amorphous alloy/Al MMCs. The wear track's width and wear volume of the 316L/Al MMCs decreased with the increase in the 316L particles areal density of the MMCs surface. The wear volume of 316L/Al MMCs was only 14–44% of that of the untreated AL substrate.

In order to conduct an in-depth study of the wear mechanisms, the microstructures of the worn surfaces were examined. It was found that only a small quantity of Fe-based amorphous alloy particles was worn and there were a large number of parallel furrows on the worn surface, as shown in Fig. 17(a). This indicated that in the Fe-based amorphous alloy/Al MMCs the wear mechanism was abrasive wear. On the worn surface of the 316L/Al MMCs, both the 316L stainless steel particles and aluminum substrate were worn, a large number of furrows and residual particles were generated (Fig. 17b), and the width of the wear tracks had increased (Fig. 17h). The wear of the untreated aluminum substrate was severe, the furrows generated on the worn surface were very wide, and there were delamination and debris caused by adhesive wear (Ref 55), as shown in Fig. 17(f). After analyzing the wear morphology of MMCs with different 316L particles areal densities, it was found that with an increase in the powder feed rate the areal density of the particles on the MMCs surface increased and the wear volume of the MMCs decreased, after wear, as shown in Fig. 16.

The main reasons for the different wear results are as follows. After implantation of hard particles into the surface of the substrate, the high-speed impact of the particles caused severe plastic deformation of the substrate, generating a large number of dislocations and leading to an increase in the substrate microhardness, improving the wear resistance of the substrate (Ref 19, 52). However, since the untreated aluminum substrate did not introduce hard particles, it also underwent severe adhesive wear, in addition to abrasive wear. After the hard particles were implanted into the substrate, during the wear process the hard particles on the surface of the substrate prevented contact between the friction pair and the substrate, consequentially preventing friction pairs from penetrating and cutting deeply into the soft aluminum surface and thereby improving the wear resistance of the substrate. Moreover, with an increase in hardness of the implanted particles, their ability to resist plastic deformation increased, leading to better wear resistance. Therefore, only a small amount of Fe-based amorphous alloy particles underwent wear in the case of Fe-based amorphous alloy/Al MMCs and the substrate remained almost intact.

Strengthening Mechanism

High-speed particle implantation for the preparation of MMCs can effectively introduce shot peening and metal matrix composite strengthening, which is the double-strengthening effect. It can be found through simulation that the high-speed impact of particles on the substrate causes severe plastic deformation of the substrate, resulting in high strain rate deformation and an increase in the temperature at the interface between the particles and the substrate, as shown in Fig. 18(b). A high strain rate deformation leads to a significant increment in dislocation density and dislocation due to the dislocation cross-slip, dislocation climb, and new grain growth (Ref 53). Furthermore, it greatly improves the surface hardness of the substrate and can effectively increase the wear resistance of the substrate. In situ grain refinement at the interface region of the particle and substrate was frequently observed, which has been demonstrated to result from the dynamic

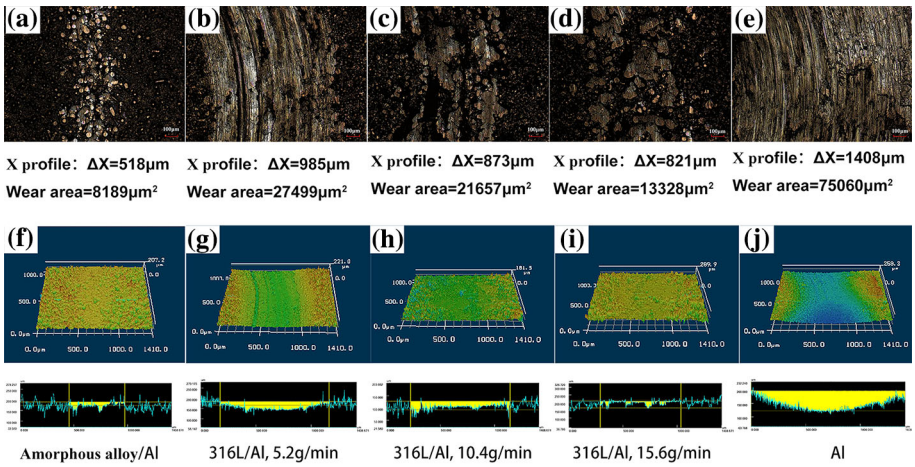

Fig. 15 The morphologies after wear test: (a) and (f) are laser photograph and 3D morphology of the amorphous alloys/Al MMCs; (b) and (g) are laser photograph and 3D morphology of the 316L/Al MMCs, powder feeding rate is 5.2 g/min; (c) and (h) are laser photograph and 3D morphology of the 316L/Al MMCs, powder feeding rate is 10.4 g/min; (d) and (i) are laser photograph and 3D morphology of the 316L/Al MMCs, powder feeding rate is 15.6 g/min; (e) and (j) are laser photograph and 3D morphology of aluminum

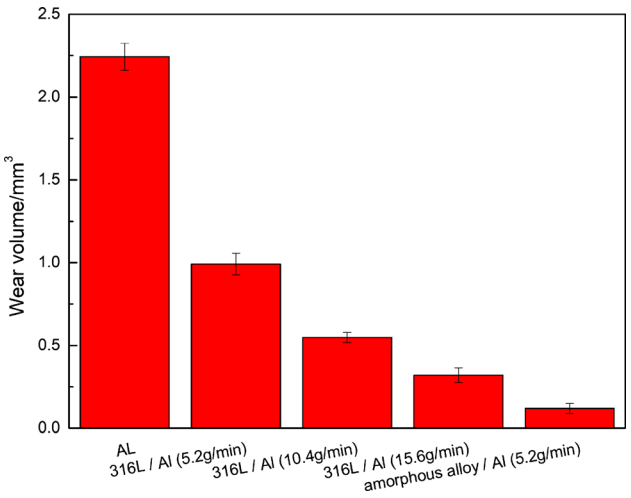

Fig. 16 Wear volume of MMCs and untreated aluminum after wear test

recrystallization that occurs during particle impacting (Ref 52), which can improve the substrate hardness (Ref 56).

During particle implantation, the particles were implanted into the substrate in a solid state due to the low processing temperature so that quenching stresses could be avoided. The 316L stainless steel and Fe-based amorphous alloy had lower CTE than the aluminum substrates, and thus, the thermal stresses were compressive. Therefore, in particle implantation, peening stress dominates the residual stress state and compressive residual stress is expected because of the high particle velocity impact (shown in Fig. 18c), which can effectively improve the fatigue wear resistance and fatigue life of the substrate (Ref 52, 57).

In addition, the formed MMCs can be strengthened via introduction of reinforcing phase particles. The reinforcing phase particles prevent the hard friction pair from cutting into the soft substrate and causing severe wear to the substrate. Therefore, the method of preparing MMCs on the surface of the substrate via high-speed particle implantation can simultaneously achieve shot peening and metal matrix composite strengthening, that is, the double-strengthening effect.

Laser-Assisted Particle Implantation

The thickness of MMCs prepared by particle implantation is limited. In order to increase the thickness of MMCs, a laser was used to preheat the substrate during the particle implantation process, that is, laser-assisted particle implantation. The substrate was zinc, and the particles were WC and Cr. The experimental results are shown in Fig. 19. It was found that the thickness of the prepared MMCs varied with laser power. As the laser power increased, the substrate absorbed more energy and the thickness of the molten substrate, the depth of particle implantation, and the thickness of the formed MMCs increased. When the laser power was 700 W, the thickness of the prepared Cr/Zn and WC/Zn MMCs was 0.89 mm and 1.25 mm, respectively. The reinforcing phase particles were uniformly dispersed in the composite material, as shown in Fig. 20. Therefore, the use of laser-assisted particle implantation can effectively pre-treat the required MMCs. By adjusting the power of the laser and the action time of the laser on the substrate, the melting depth of the substrate can be adjusted to prepare a MMCs material with the desired thickness.

In the preparation of MMCs via laser-assisted particle implantation, the double-strengthening effect of metal matrix composite strengthening and the grain refinement effect can improve the MMC's wear resistance. The

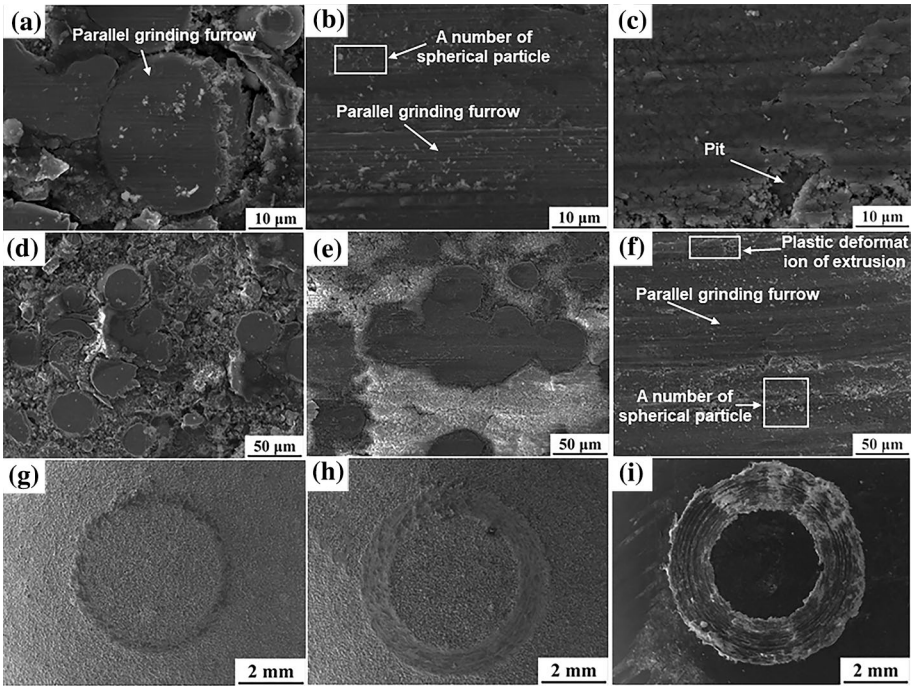

Fig. 17 SEM images of untreated aluminum substrate and MMCs after wearing: (a), (d), (g) amorphous alloys/Al MMCs, powder feeding rate is 5.2 g/min; (b), (e), (h) 316L/Al MMCs, powder feeding rate is 5.2 g/min; (c), (f), (i) untreated aluminum substrate

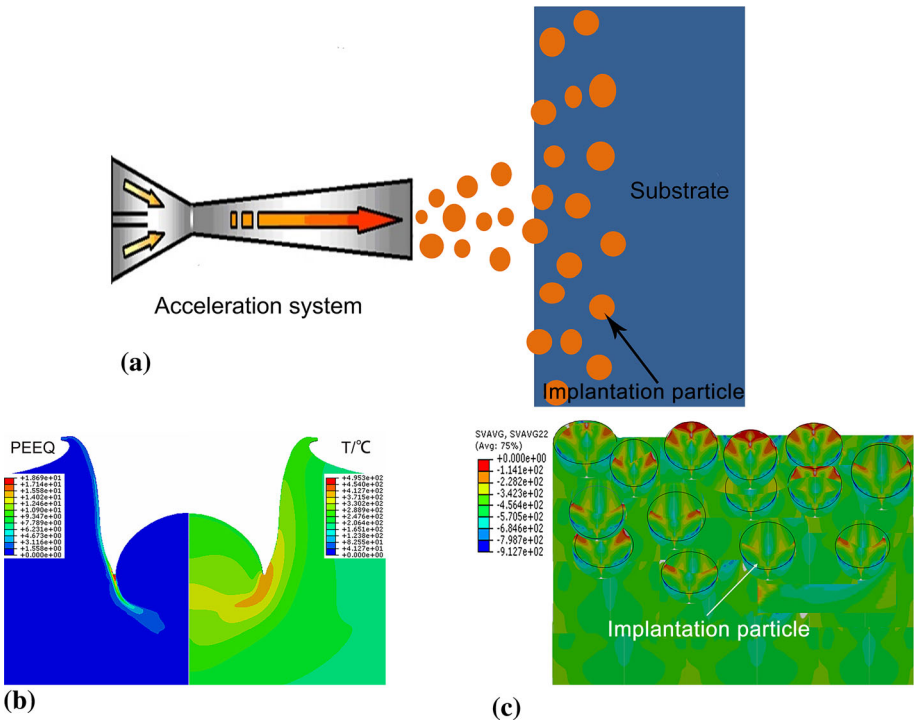

Fig. 18 (a) Schematic diagram of particles implantation; (b) contours of the effective plastic stain (PEEQ) (left) and temperature (right) after a 316L stainless steel particle impacting on an Al substrate; (c) stress distribution in MMCs after high-speed particle implantation

dispersion distribution of the hard phase particles can strengthen MMCs; the lattice distortion and stress field at the interface between the metal substrate and the hard particles will become an obstacle for dislocation movement in the metal substrate under the action of external stress and the macroscopic performance is the significant strengthening of MMCs. Moreover, grain refinement can occur due to the high heating and cooling speed achieved with the introduction of a laser, leading to an increase in substrate hardness (Ref 13).

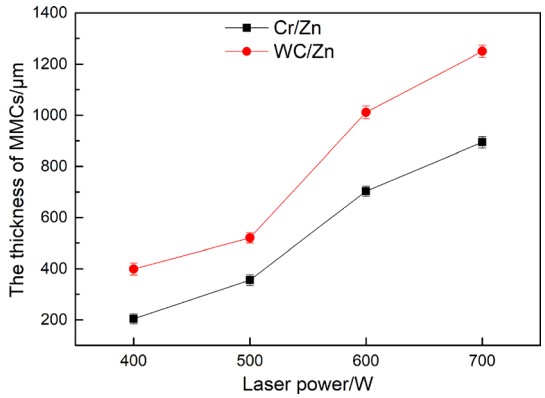

Fig. 19 Trend of the thickness of MMCs with laser power

Conclusions

This study demonstrated the method of preparation of MMCs via high-speed particle implantation. Through the combination of experiments and simulations, it was demonstrated that MMCs can simultaneously achieve shot peening and metal matrix composite strengthening, that is, the double-strengthening effect. This MMCs surface can effectively protect the aluminum substrate and improve its wear resistance. The introduction of a laser can increase the MMCs thickness. The main conclusions of this study are as follows:

Through simulation, it was found that the properties of materials and the kinetic energy of particles have important effects on particle implantation. A decrease in yield strength, elastic modulus, and an increase in kinetic energy can improve the plastic deformation of the substrate and increase the particle implantation depth. Preheating the substrate and multi-particle implantation can also promote particle implantation, resulting in an increase in the particle implantation depth.

The formation of MMCs on the aluminum substrate surface can improve the wear resistance of the aluminum substrate. The wear volume of the wear tracks on the aluminum substrate decreased sharply after the implantation of the hard particles. The untreated aluminum substrate underwent severe wear, and the wear volume was approximately 19 times greater than that of the Fe-based amorphous alloy/Al MMCs. The wear volume of the 316L/Al MMCs decreased with an increase in the areal density of 316L particles on the surface of the MMCs. The wear volume of 316L/Al MMCs was only 14–44% of that of the untreated aluminum substrate.

The introduction of a laser can increase the MMCs thickness. By adjusting the power of the laser and the action time of the laser on the substrate, a MMCs material can be prepared with the desired thickness.

The double-strengthening effect can be introduced in high-speed particle implantation for preparation of MMCs. High-speed particle implantation leads to the substrate undergoing more severe plastic deformation and introduces shot peening strengthening. This results in an increase in dislocation density and in situ grain refinement, which can significantly improve the surface hardness of the substrate and effectively increase the wear resistance of the substrate. Moreover, compressive residual stress is introduced due to the high particle velocity impact, which can effectively improve the fatigue wear resistance and fatigue life of the substrate. In addition, the formed MMCs can be strengthened via the introduction of reinforcing phase particles. The reinforcing phase particles can prevent the hard friction pair from cutting into the soft substrate, reducing the wear of the substrate.

In conclusion, preparation of MMCs via high-speed particle implantation can effectively improve the wear resistance of soft substrates due to the double-strengthening

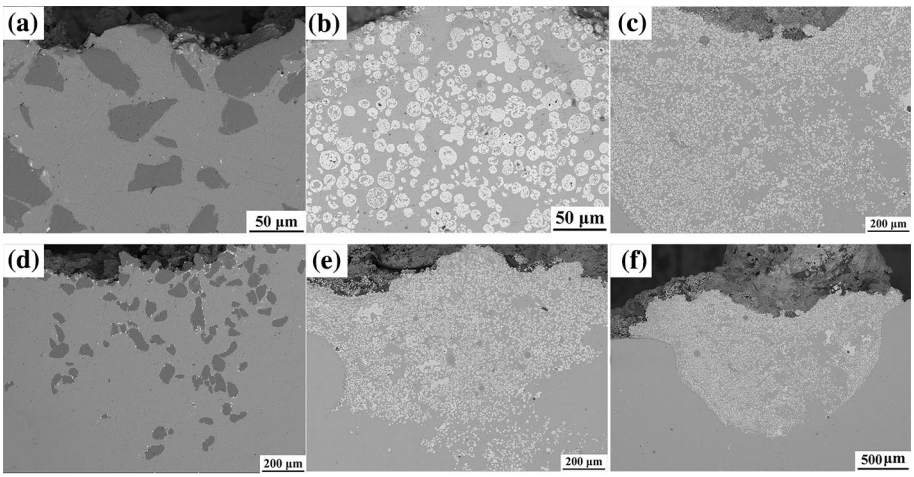

Fig. 20 SEM images of MMCs: (a) and (d) Cr/Zn, 700 W; (b) and (e) WC/Zn, 600 W; (c) and (f) WC/Zn, 700 W

effect. The introduction of a laser can be used to adjust and prepare a MMCs material with the desired thickness.

Acknowledgements This work was supported by the National Natural Science Foundation of China (No. 51761145108).

References

1. D. He, G. Li, D. Shen, C. Guo, H. Ma, and J. Cai, Effect Mechanism of Ultrasound on Growth of Micro-Arc Oxidation Coatings on A96061 Aluminum Alloy, *Vacuum*, 2014, **107**, p 99-102. https://doi.org/10.1016/j.vacuum.2014.04.015
2. A.H. Wang, C.S. Xie, and W.Y. Wang, Cracking Behavior in the Transitional Region of Laser-Clad Coatings on Al-Si Alloy under Multiple Impact Loading, *Mater. Charact.*, 2002, **49**(3), p 247-254
3. G.Y. Liang and T.T. Wong, Microstructure and Character of Laser Remelting of Plasma Sprayed Coating (Ni-Cr-B-Si) on Al-Si Alloy, *Surf. Coat. Technol.*, 1997, **89**(1–2), p 121-126
4. T. Wei, F. Yan, and J. Tian, Characterization and Wear- and Corrosion-Resistance of Microarc Oxidation Ceramic Coatings on Aluminum Alloy, *J. Alloys Compd.*, 2005, **389**(1–2), p 169-176
5. P. Kadolkar and N.B. Dahotre, Variation of structure with input energy during laser surface engineering of ceramic coatings on aluminum alloys, *Appl Surf Sci*, 2002, **199**, p 222-233
6. J. Zhou, K. Ma, C.X. Li, M. Yasir, X.T. Luo, and C.J. Li, Microstructures of Aluminum Surfaces Reinforced with 316L Stainless Steel Particles via High-Speed Particle Injection and the Resulting Double-Strengthening Mechanism, *Surf. Coat. Technol.*, 2020, **385**, p 125380. https://doi.org/10.1016/j.surfcoat.2020.125380
7. A. Pramanik and G. Littlefair, Fabrication of Nano-particle Reinforced Metal Matrix Composites, *Adv. Mater. Res.*, 2013, **651**, p 289-294. https://doi.org/10.4028/www.scientific.net/AMR.651.289
8. M. Ibrahim, A. El, and H. Seop, Wear Properties of High Pressure Torsion Processed Ultrafine Grained Al–7% Si Alloy, *Mater. Des.*, 2014, **53**, p 373-382. https://doi.org/10.1016/j.matdes.2013.07.045
9. A. Sova, S. Grigoriev, A. Okunkova, and I. Smurov, Cold Spray Deposition of 316L Stainless Steel Coatings on Aluminium Surface with Following Laser Post-Treatment, *Surf. Coat. Technol.*, 2013, **235**, p 283-289
10. P. Fu, K. Zhan, and C. Jiang, Micro-Structure and Surface Layer Properties of 18CrNiMo7-6 Steel after Multistep Shot Peening, *Mater. Des.*, 2013, **51**, p 309-314. https://doi.org/10.1016/j.matdes.2013.04.011
11. F. Yang, Z. Chen, and S.A. Meguid, Effect of Initial Surface Finish on Effectiveness of Shot Peening Treatment Using Enhanced Periodic Cell Model, *Int. J. Mech. Mater. Des.*, 2015, **11**(4), p 463-478. https://doi.org/10.1007/s10999-014-9273-y
12. M. Hosseini and H.D. Manesh, Immersed Friction Stir Welding of Ultrafine Grained Accumulative Roll-Bonded Al Alloy, *Mater. Des.*, 2010, **31**(10), p 4786-4791
13. X. Li, Z. Liu, and Y. Wang, Microstructure and Corrosion Properties of Laser Cladding MoNi Based Alloy Coatings, *Sci. China Technol. Sci.*, 2014, **57**(5), p 980-989
14. A. Pramanik, Effects of Reinforcement on Wear Resistance of Aluminum Matrix Composites, *Trans. Nonferrous Met. Soc. China (English Ed.)*, 2016, **26**(2), p 348-358
15. X. Guo, J. Chen, H. Yu, H. Liao, and C. Coddet, A Study on the Microstructure and Tribological Behavior of Cold-Sprayed Metal Matrix Composites Reinforced by Particulate Quasicrystal, *Surf. Coat. Technol.*, 2015, **268**, p 94-98
16. S. Yin, Z. Zhang, E.J. Ekoi, J. Jing, D.P. Dowling, V. Nicolosi, and R. Lupoi, Novel Cold Spray for Fabricating Graphene-Reinforced Metal Matrix Composites, *Mater. Lett.*, 2017, **196**, p 172-175. https://doi.org/10.1016/j.matlet.2017.03.018
17. X. Xie, Y. Ma, C. Chen, G. Ji, C. Verdy, H. Wu, Z. Chen, S. Yuan, B. Normand, S. Yin, and H. Liao, Cold Spray Additive Manufacturing of Metal Matrix Composites (MMCs) Using a Novel Nano-TiB2-Reinforced 7075Al Powder, *J. Alloys Compd.*, 2020. https://doi.org/10.1016/j.jallcom.2019.152962
18. R.C. Dykhuizen and M.F. Smith, Gas Dynamic Principles of Cold Spray, *J. Therm. Spray Technol.*, 1998, **7**(2), p 205-212
19. W. Li, K. Yang, D. Zhang, and X. Zhou, Residual Stress Analysis of Cold-Sprayed Copper Coatings by Numerical Simulation, *J. Therm. Spray Technol.*, 2016, **25**(1–2), p 131-142
20. C. García-Cordovilla, J. Narciso, and E. Louis, Abrasive Wear Resistance of Aluminium Alloy/Ceramic Particulate Composites, *Wear*, 1996, **192**(1–2), p 170-177
21. P. Suwannaroop, P. Chaijareenont, N. Koottathape, H. Takahashi, and M. Arksornnukit, In Vitro Wear Resistance, Hardness and Elastic Modulus of Artificial Denture Teet, *Dent. Mater. J.*, 2011, **30**(4), p 461-468. https://doi.org/10.4012/dmj.2010-200
22. Y.K. Wei, X.T. Luo, C.X. Li, and C.J. Li, Optimization of In-Situ Shot-Peening-Assisted Cold Spraying Parameters for Full Corrosion Protection of Mg Alloy by Fully Dense Al-Based Alloy Coating, *J. Therm. Spray Technol.*, 2017, **26**(1–2), p 173-183
23. J. Wang, Q. Jia, X. Yuan, and S. Wang, Applied Surface Science Experimental Study on Friction and Wear Behaviour of Amorphous Carbon Coatings for Mechanical Seals in Cryogenic Environment, *Appl. Surf. Sci.*, 2012, **258**(24), p 9531-9535. https://doi.org/10.1016/j.apsusc.2012.05.103
24. C. Chen, Y. Xie, S. Yin, M. Planche, and S. Deng, Evaluation of the Interfacial Bonding between Particles and Substrate in Angular Cold Spray, *Mater. Lett.*, 2016, **173**, p 76-79. https://doi.org/10.1016/j.matlet.2016.03.036
25. S. Dosta, G. Bolelli, A. Candeli, L. Lusvarghi, I. Garcia, and J. Maria, Acta Materialia Plastic Deformation Phenomena during Cold Spray Impact of WC-Co Particles onto Metal Substrates, *Acta Mater.*, 2017, **124**, p 173-181. https://doi.org/10.1016/j.actamat.2016.11.010
26. M. Grujicic, C.L. Zhao, W.S. DeRosset, and D. Helfritch, Adiabatic Shear Instability Based Mechanism for Particles/Substrate Bonding in the Cold-Gas Dynamic-Spray Process, *Mater. Des.*, 2004, **25**(8), p 681-688
27. F.F. Wang, W.Y. Li, M. Yu, and H.L. Liao, Prediction of Critical Velocity during Cold Spraying Based on a Coupled Thermomechanical Eulerian Model, *J. Therm. Spray Technol.*, 2014, **23**(1–2), p 60-67
28. M. Yu, W.Y. Li, F.F. Wang, and H.L. Liao, Finite Element Simulation of Impacting Behavior of Particles in Cold Spraying by Eulerian Approach, *J. Therm. Spray Technol.*, 2012, **21**(3–4), p 745-752
29. W.Y. Li and W. Gao, Some Aspects on 3D Numerical Modeling of High Velocity Impact of Particles in Cold Spraying by Explicit Finite Element Analysis, *Appl. Surf. Sci.*, 2009, **255**(18), p 7878-7892
30. S. Yin, X.F. Wang, B.P. Xu, and W.Y. Li, Examination on the Calculation Method for Modeling the Multi-Particle Impact Process in Cold Spraying, *J. Therm. Spray Technol.*, 2010, **19**(5), p 1032-1041
31. W.Y. Li, H. Liao, C.J. Li, H.S. Bang, and C. Coddet, Numerical Simulation of Deformation Behavior of Al Particles Impacting on Al Substrate and Effect of Surface Oxide Films on Interfacial Bonding in Cold Spraying, *Appl. Surf. Sci.*, 2007, **253**(11), p 5084-5091

32. T.S. Price, P.H. Shipway, and D.G. Mccartney, Effect of Cold Spray Deposition of a Titanium Coating on Fatigue Behavior of a Titanium Alloy, *J. Therm. Spray Technol.*, 2006, **15**(December), p 507-512
33. S. Rech, A. Trentin, S. Vezzù, J.G. Legoux, E. Irissou, and M. Guagliano, Influence of Pre-Heated Al 6061 Substrate Temperature on the Residual Stresses of Multipass Al Coatings Deposited by Cold Spray, *J. Therm. Spray Technol.*, 2011, **20**(1–2), p 243-251
34. D.K. Christoulis, S. Guetta, V. Guipont, and M. Jeandin, The Influence of the Substrate on the Deposition of Cold-Sprayed Titanium: An Experimental and Numerical Study, *J. Therm. Spray Technol.*, 2011, **20**(3), p 523-533
35. G. Ma, X. Cui, Y. Shen, C. Nuria, J.M. Guilemany, and T. Xiong, Influence of Substrate Mechanical Properties on Deposition Behaviour of 316L Stainless Steel Powder, *Jinshu Xuebao/Acta Metall. Sin.*, 2016, **52**(12), p 1610-1618
36. S. Kumar, G. Bae, and C. Lee, Influence of Substrate Roughness on Bonding Mechanism in Cold Spray, *Surf. Coatings Technol.*, 2016, **304**, p 592-605. https://doi.org/10.1016/j.surfcoat.2016.07.082
37. G. Bae, Y. Xiong, S. Kumar, K. Kang, and C. Lee, General Aspects of Interface Bonding in Kinetic Sprayed Coatings, *Acta Mater.*, 2008, **56**(17), p 4858-4868
38. X.M. Meng, J.B. Zhang, W. Han, and J. Zhao, Numerical and Experimental Investigation on Effect of Impact Velocity on Particle Deposition Characteristics in Cold Spraying, *Mater. Res. Innov.*, 2011, **15**(4), p 283-289
39. W.Y. Li, H. Liao, C.J. Li, G. Li, C. Coddet, and X. Wang, On High Velocity Impact of Micro-Sized Metallic Particles in Cold Spraying, *Appl. Surf. Sci.*, 2006, **253**(5), p 2852-2862
40. H. Assadi, F. Gärtner, T. Stoltenhoff, and H. Kreye, Bonding Mechanism in Cold Gas Spraying, *Acta Mater.*, 2003, **51**(15), p 4379-4394
41. P. Zhang and J. Lindemann, Influence of Shot Peening on High Cycle Fatigue Properties of the High-Strength Wrought Magnesium Alloy AZ80, *Scr. Mater.*, 2005, **52**(6), p 485-490
42. R. Ghelichi, S. Bagherifard, M. Guagliano, and M. Verani, Numerical Simulation of Cold Spray Coating, *Surf. Coat. Technol.*, 2011, **205**(23–24), p 5294-5301. https://doi.org/10.1016/j.surfcoat.2011.05.038
43. S. Yin, X. Suo, J. Su, Z. Guo, H. Liao, and X. Wang, Effects of Substrate Hardness and Spray Angle on the Deposition Behavior of Cold-Sprayed Ti Particles, *J. Therm. Spray Technol.*, 2014, **23**(1–2), p 76-83
44. S. Yin, X. Wang, X. Suo, H. Liao, Z. Guo, and W. Li, Deposition Behavior of Thermally Softened Copper Particles in Cold Spraying, *Acta Mater.*, 2013, **61**(14), p 5105-5118. https://doi.org/10.1016/j.actamat.2013.04.041
45. M. Yu, W.Y. Li, F.F. Wang, X.K. Suo, and H.L. Liao, Effect of Particle and Substrate Preheating on Particle Deformation Behavior in Cold Spraying, *Surf. Coat. Technol.*, 2013, **220**, p 174-178
46. J. Hünecke, D. Schöne, D. Klingbeil, and C.P. Bork, Advanced Life Prediction by Microstructural Simulation of Short Cracks in a Low Carbon Steel, *Int. J. Fatigue*, 2006, **28**(9), p 993-1000
47. C.J. Li and W.Y. Li, Deposition Characteristics of Titanium Coating in Cold Spraying, *Surf. Coat. Technol.*, 2003, **167**(2–3), p 278-283
48. G. Bae, S. Kumar, S. Yoon, K. Kang, H. Na, H.J. Kim, and C. Lee, Bonding Features and Associated Mechanisms in Kinetic Sprayed Titanium Coatings, *Acta Mater.*, 2009, **57**(19), p 5654-5666. https://doi.org/10.1016/j.actamat.2009.07.061
49. G. Bae, K. Kang, J.J. Kim, and C. Lee, Nanostructure Formation and Its Effects on the Mechanical Properties of Kinetic Sprayed Titanium Coating, *Mater. Sci. Eng. A*, 2010, **527**(23), p 6313-6319
50. U. Prisco, Size-Dependent Distributions of Particle Velocity and Temperature at Impact in the Cold-Gas Dynamic-Spray Process, *J. Mater. Process. Technol.*, 2015, **216**, p 302-314. https://doi.org/10.1016/j.jmatprotec.2014.09.013
51. W. Li, C. Zhang, X. Guo, and C. Li, Study on Impact Fusion at Particle Interfaces and Its Effect on Coating Microstructure in Cold Spraying, *Appl Surf Sci*, 2007, **254**, p 517-526
52. X.T. Luo, C.X. Li, F.L. Shang, G.J. Yang, Y.Y. Wang, and C.J. Li, High Velocity Impact Induced Microstructure Evolution during Deposition of Cold Spray Coatings: A Review, *Surf. Coatings Technol.*, 2014, **254**, p 11-20. https://doi.org/10.1016/j.surfcoat.2014.06.006
53. K. Zhu and X. Yu, The Monitoring of Micro Milling Tool Wear Conditions by Wear Area Estimation, *Mech. Syst. Signal Process.*, 2017, **93**, p 80-91. https://doi.org/10.1016/j.ymssp.2017.02.004
54. R. Gecu, H. Atapek, and A. Karaaslan, Influence of Preform Preheating on Dry Sliding Wear Behavior of 304 Stainless Steel Reinforced A356 Aluminum Matrix Composite Produced by Melt Infiltration Casting, *Tribol. Int.*, 2017, **115**(June), p 608-618. https://doi.org/10.1016/j.triboint.2017.06.040
55. P. Ravindran, K. Manisekar, S.V. Kumar, and P. Rathika, Investigation of Microstructure and Mechanical Properties of Aluminum Hybrid Nano-Composites with the Additions of Solid Lubricant, *Mater. Des.*, 2013, **51**, p 448-456
56. H. Luong and M.R. Hill, The Effects of Laser Peening on High-Cycle Fatigue in 7085-T7651 Aluminum Alloy, *Mater. Sci. Eng. A*, 2008, **477**(1–2), p 208-216
57. T. Suhonen, T. Varis, S. Dosta, M. Torrell, and J.M. Guilemany, Residual Stress Development in Cold Sprayed Al, *Cu and Ti Coatings, Acta Mater.*, 2013, **61**(17), p 6329-6337. https://doi.org/10.1016/j.actamat.2013.06.033